



1 **Do alternative inventories converge on the spatiotemporal representation of spring**
2 **ammonia emissions in France?**

3 Audrey Fortems-Cheiney^{1,*}, Gaëlle Dufour¹, Karine Dufossé^{2,**}, Florian Couvidat³, Jean-
4 Marc Gilliot², Guillaume Siour¹, Matthias Beekmann¹, Gilles Foret¹, Frederik Meleux³,
5 Lieven Clarisse⁴, Pierre-François Coheur⁴, Martin Van Damme⁴, Cathy Clerbaux^{4,5} and
6 Sophie Générumont²

7 ¹Laboratoire Interuniversitaire des Systèmes Atmosphériques, UMR CNRS 7583, Université
8 Paris Est Créteil et Université de Paris, Institut Pierre Simon Laplace, Créteil, France.

9 ²Université Paris-Saclay, INRAE, AgroParisTech, UMR ECOSYS,78850Thiverval-Grignon,
10 France.

11 ³Institut National de l'Environnement Industriel et des Risques, INERIS, 60550 Verneuil en
12 Halatte, France.

13 ⁴Université libre de Bruxelles, Spectroscopy, Quantum Chemistry and Atmospheric Remote
14 Sensing (SQUARES), Brussels, Belgium.

15 ⁵LATMOS/IPSL, Sorbonne Université, UVSQ, CNRS, Paris, France.

16 *now at Laboratoire des Sciences du Climat et de l'Environnement, LSCE-IPSL (CEA-
17 CNRS-UVSQ), Université Paris-Saclay, 91191 Gif-sur-Yvette, France.

18 **now at UniLaSalle - Ecole des Métiers de l'Environnement, Rennes, France.

19

20 **Abstract**

21 Agriculture is the main source of ammonia (NH₃) in France, an important gaseous precursor
22 of atmospheric particulate matter (PM). National and even more global emission inventories
23 are known to have difficulty representing the large spatial and temporal variability inherent to
24 atmospheric NH₃. In this study, we compare NH₃ emissions in France during the spring 2011
25 from (i) one reference inventory, the TNO inventory, and two alternative inventories that
26 account in different manners for both the spatial and temporal variabilities of the emissions
27 (ii) the NH₃SAT satellite-derived inventory based on IASI NH₃ columns and (iii) the
28 CADASTRE-CIT inventory that combines NH₃ emissions due to nitrogen fertilization
29 calculated with the mechanistic model VOLT'AIR on the database of the CADASTRE_NH₃
30 framework and other source emissions from the CITEPA. The total spring budgets at the
31 national level are higher when calculated with both alternative inventories than with the
32 reference, the difference being more marked with CADASTRE-CIT. NH₃SAT and



33 CADASTRE-CIT inventories both yield to large NH_3 emissions due to fertilization on soils
34 with high pH in the northeastern part of France (65 kt NH_3 and 135 kt NH_3 , respectively, vs 48
35 kt NH_3 for TNO-GEN), while soil properties are not accounted for by the TNO-GEN
36 methodology. For the other parts of France, the differences are smaller. The timing of
37 fertilization and associated ammonia emissions is closely related to the nitrogen requirements
38 and hence the phenological stage of the crops, and therefore to the crop-year's specific weather
39 conditions. Maximum emissions are observed in March for 2011 for some regions for both
40 alternative inventories, while April is the period with maximum emissions for the reference
41 inventory whatever the region or the year. Comparing the inventories at finer temporal
42 resolutions, typically at daily scale, large differences are found. The convergence of
43 alternative, independent and complementary methods on the spatiotemporal representation of
44 the spring NH_3 emissions particularly over areas where the contribution of mineral fertilizer
45 spreading to the spring budget is strong, encouraging further developments in both prospected
46 complementary directions, as this will help improving national NH_3 emission inventories.

47

48 1. Introduction

49 France is a major crop producer and a major exporter of agricultural and food products. In
50 2014, it produced 2%, 4%, 5%, 8%, 8% and 14% of the global production of maize,
51 sunflower, wheat, barley, rapeseed and sugar beet, respectively [Food and Agriculture
52 Organization of the United Nations FAO, Schauburger et al., 2018]. Through this food
53 cultivation and also due to animal husbandry, agriculture is the main source of ammonia
54 (NH_3) in the country. As an important gaseous precursor of particulate pollution, harmful to
55 human life [Lelieveld et al., 2015; WHO, 2016], ammonia plays an important role in the
56 regulation of inorganic aerosol concentrations [Erisman and Schaap, 2004, Bauer et al.,
57 2016], and contributes to N deposition and potential exceedance of critical loads of
58 ecosystems [Erisman et al., 2007; EEA European Environment Agency, 2014]. In order to
59 limit air pollution, also responsible for acidification and eutrophication, the new European
60 National Emission Ceilings Directive 2016/2284, replacing the Directive 2001/81/EC, now
61 sets ambitious national reduction commitments for ammonia. Ammonia emissions indeed
62 have to be reduced by 19% in 2030, compared with the 2005 levels [OJEU, 2016].

63

64 At the European scale, total NH_3 emissions are provided by the European Monitoring and
65 Evaluation Program (EMEP) [Vestreng, 2005] or by the TNO-MACCI3 [Kuenen et al., 2014]



66 inventories that rely on national annual declarations and estimates of emission factors.
67 Emissions are accounted for without separating fertilization and livestock. These reference
68 inventories are widely used by the scientific community to study the impact of pollutant
69 emissions on the chemical composition of the troposphere and on air quality. Nevertheless,
70 uncertainties on the quantification of the NH_3 emissions are usually estimated to be between
71 100 and 300% of the annual budgets in the reference inventories [EMEP/EEA, 2016; Kuenen
72 et al., 2014]. In addition, the temporal and spatial variability may be not well represented in
73 the reference inventories, as the temporal profiles used do not account for meteorology, soil
74 properties and other local conditions. Moreover, fertilizer spreading is of particular interest,
75 as these are applied during small periods, especially during a few weeks at the end of winter
76 and early spring. However, the exact timing of fertilizer spreading is difficult to predict, as it
77 depends on agricultural practices and meteorological conditions, which is not taken into
78 account in the temporal disaggregation of the reference emission inventories. Both the
79 inaccurate temporal resolutions and the mis-representation of the spreading emissions largely
80 explain the difficulty encountered by models to represent seasonal or daily pattern of NH_3
81 concentrations [Menut et al., 2012], and consequently particulate matter levels [Fortems-
82 Cheiney et al, 2016].

83
84 To reduce these uncertainties, a better quantification of agricultural ammonia emissions and
85 its time and spatial evolution is necessary. In particular, one of the challenges is to capture the
86 right timing of fertilizer spreading at the weekly or even at the daily scale in order to reflect
87 the effect of environmental and agronomical conditions on ammonia emissions. To this end,
88 mechanistic models taking into account meteorological conditions, soil properties and
89 agricultural practices, have been developed (e.g., for Denmark [Skjøth et al., 2004], for the
90 UK [Hellsten et al., 2008], and for mineral fertilization in springtime in France [Hamaoui-
91 Laguel et al., 2014]). Limitations for such approaches come from the fact that detailed
92 agricultural data needed as input to such models are not available for most of the European
93 countries. Moreover, agricultural practices of a specific country cannot be extrapolated to
94 another country [Skjøth et al., 2011].

95
96 As an alternative to direct emission modeling, attempts have been made to constrain ammonia
97 emissions through inverse approaches, based on satellite observed atmospheric ammonia
98 distributions (e.g., from the Tropospheric Emission Spectrometer TES [Zhu et al., 2013], from
99 the Infrared Atmospheric Sounding Interferometer (IASI) [Fortems-Cheiney et al., 2016; Van



100 Damme et al., 2018; Adams et al., 2019] or from the Cross-track Infrared Sounder CrIS
101 [Adams et al., 2019; Dammers et al., 2019]). In principle, such emission estimates can be
102 available shortly after observation. The advantage of satellite-derived estimates is also that
103 these can be derived globally, at a high temporal scale (e.g., daily scale under clear sky). The
104 downside of these however, is that they do not provide information on the underlying sources
105 of the emissions (fertilizers vs husbandry), or e.g. the date of fertilization, the type of
106 fertilizers used, the fertilization rates, etc., that could be important for the regulation of NH₃
107 emissions.

108

109 In this context, we compare ammonia emissions in France from inventories using the different
110 approaches mentioned above: (i) the reference, hereafter called TNO-GEN, is the European
111 inventory based on the annual budgets provided by the TNO-MACCI3 inventory [Kuenen et
112 al., 2014] and seasonal profiles from GENEMIS [Ebel et al., 1997], (ii) a first alternative
113 inventory, hereafter called NH₃SAT, is based on a top-down approach starting from the IASI
114 derived NH₃ columns ; (iii) the other alternative inventory, hereafter called CADASTRE-CIT,
115 is based on a bottom-up approach quantifying NH₃ emissions due to nitrogen fertilization
116 combining spatiotemporal data and calculations performed within the CADASTRE_NH₃
117 framework with the mechanistic model VOLT'AIR ([Ramanantenasoa et al., [2018];
118 Générumont et al., [2018]) completed with livestock and other source emissions from the
119 French Interprofessional Technical Centre for Studies on Air Pollution (CITEPA). This study
120 aims at assessing the potential contribution of better spatial and temporal representation of
121 fertilization-related ammonia emissions to the quality of ammonia emission inventories. The
122 improvement is assessed in terms of total budget, spatial distribution and timing of the
123 emissions. The study period, spring 2011 (from March to May 2011), was chosen following
124 three criteria. Firstly, because at the time of the study, the last French agricultural data were
125 available from AGRESTE [AGRESTE, 2014] for the agricultural year 2010-2011, allowing
126 the application of the CADASTRE_NH₃ framework for the quantification of the spatio-
127 temporal distribution of NH₃ emissions due to nitrogen fertilization for this crop year
128 [Ramanantenasoa et al., 2018; Générumont et al., 2018]. Secondly, ammonia emissions are
129 enhanced during spring in accordance with N crops requirements [Skjøth et al., 2004;
130 Ramanantenasoa et al., 2018; Générumont et al., 2018]. Finally, unlike autumn and winter
131 months, the NH₃ spring levels are detectable with a better confidence in the IASI satellite
132 observations [Viatte et al., 2020], allowing the extension of the preliminary work of Fortems-
133 Cheiney et al. [2016] to deduce NH₃ emissions from the IASI satellite instrument.



134 The three inventories and methods to build them used for this study are presented in Section 2
135 and the results of the comparison are given and discussed in Section 3.

136 2. Inventories

137 The three inventories TNO-GEN, NH₃SAT and CADASTRE-CIT compared in this study are
138 described in Table 1 and in the following sections. It is worth noting that only the
139 CADASTRE-CIT inventory provides information on the respective contribution of
140 fertilization and livestock emissions. The spatial resolutions of the inventories are also shown
141 in Table 1. The inter-comparison is made at the 0.5° (longitude) x 0.25° (latitude) resolution.
142 The outputs of the TNO-GEN and the CADASTRE-CIT inventories have consequently been
143 aggregated.

Name	Spatial Resolution (latitude x longitude)	Temporal Resolution	Fertilization emissions	Livestock emissions
TNO-GEN	0.125°x0.0625°	Monthly	-	-
NH ₃ SAT	0.5°x0.25°	Daily	-	-
CADASTRE-CIT	0.015625° x0.03125°	Hourly	CADASTRE_NH ₃ Ramanantenasoa et al., [2018] and Génermont et al., [2018]	
	0.007825°x0.007825°	Daily		CITEPA national emissions, temporalized according to Skøjth et al., [2011]

144 **Table 1.** Main characteristics of the different compared inventories.

145 2.1. TNO-GEN

146 In this study, the TNO-GEN combines the annual budgets provided by the TNO-MACCIII
147 inventory and the seasonal profiles to deduce the monthly variability of NH₃ emissions. This
148 inventory is based on official annual emission data submitted by countries to EMEP/CEIP
149 (European Monitoring and Evaluation Programme/Centre on Emission Inventories and
150 Projections) for air pollutants. It is the update of the TNO-MACCII inventory [Kuenen et al.,
151 2014]. It is an inventory at 0.125°x0.0625° resolution providing annual emissions of NH₃



152 from the agricultural sector, without separating the contributions from fertilization and
153 livestock. Hereafter, we use the TNO-MACIII emissions of year 2011. The seasonal profile of
154 these emissions is prescribed in CHIMERE according to the typical national factors provided
155 by GENEMIS. This seasonal temporal profile used for the temporalization of emissions -the
156 same one applied to the entire country- leads to a maximum in NH₃ emissions systematically
157 in April over France [Ebel et al., 1997].

158

159 **2.2. NH₃SAT**

160 As a first alternative, a mass-balance approach, which is a common method for the
161 quantification of short-lived species surface fluxes [Palmer et al., 2003; Jaeglé et al., 2004;
162 Boersma et al., 2008; Lin et al., 2010] was set-up. We used it to deduce NH₃ emissions from
163 differences between NH₃ total columns observed by the IASI instrument and simulated by the
164 CHIMERE regional chemical transport model (CTM) using the TNO-GEN inventory as
165 inputs data.

166 2.2.1 The regional CTM CHIMERE

167 CHIMERE simulates concentrations of gaseous and particulate chemical species [Menut et
168 al., 2013; Mailler et al., 2017]. For this study, we used the CHIMERE version 2013a. The
169 horizontal resolution is given as follows: $0.5^\circ \times 0.25^\circ$ over $17^\circ\text{W}/40^\circ\text{E}$ – $32^\circ\text{N}/70^\circ\text{N}$, including
170 115 (longitude) x 153 (latitude) grid-cells. The vertical grid contains 17 layers from the
171 surface to 200 hPa. This model is driven by the European Centre for Medium-Range Weather
172 Forecasts global meteorological fields [Owens and Hewson, 2018]. Climatological values
173 from the LMDZ-INCA global model [Szopa et al., 2008] are used to prescribe concentrations
174 at the lateral and top boundaries and the initial atmospheric composition in the domain. For
175 inorganic species, aerosol thermodynamic equilibrium is achieved using the ISORROPIA
176 model [Nenes et al., 1998]. The parameterization of NH₃ dry deposition is unidirectional in
177 CHIMERE.

178 2.2.2. The IASI observations

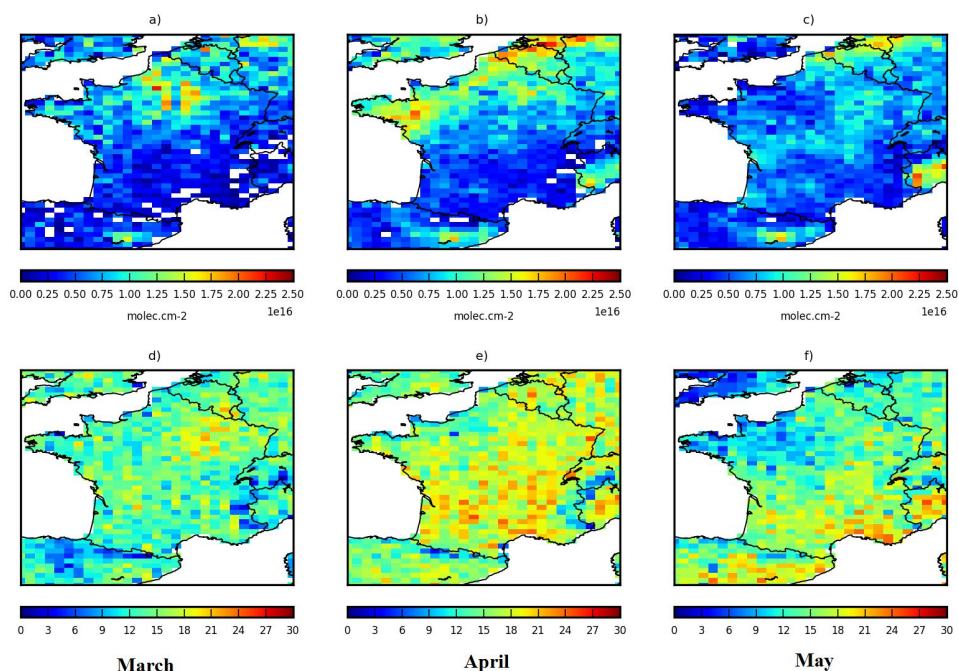
179 We use data from the IASI-A instrument, flying on a low Sun-synchronous polar orbit aboard
180 Metop satellite since October 2006, with equator crossing times of 09:30 (descending mode)
181 and 21:30 (ascending mode) local sidereal time (LST) [Clerbaux et al., 2009]. The spatial
182 resolution of its observations is about $12 \times 12 \text{ km}^2$ at nadir. The algorithm used to retrieve NH₃
183 columns from the radiance spectra is described in Van Damme et al., [2017]. Several



184 improvements have been introduced since the description of Van Damme et al., [2014] and
185 the version v1 used in our previous study [Fortems-Cheiney et al., 2016]. In this study, we use
186 the reanalyzed dataset ANNI-NH₃-v2.2R, relying on ERA-Interim meteorological input data
187 from the European Centre for Medium-Range Weather Forecasts (ECMWF) rather than the
188 operationally provided Eumetsat IASI Level 2 (L2) data used for the standard near-real-time
189 version [Van Damme et al., 2017]. We only consider land measurements from the morning
190 overpass, as IASI is more sensitive at this time to the boundary layer, owing to more
191 favorable thermal conditions [Clarisse et al., 2010, Van Damme et al., 2014].

192 The IASI total columns are averaged into “super-observations” (average of all IASI data
193 within the 0.5°×0.25° resolution of CHIMERE). As suggested by Van Damme et al. [2017],
194 we no longer use weighted averages for this purpose. We performed a sensitivity test by
195 selecting the IASI pixels for which the retrieval error does not exceed 100%: the results
196 did not significantly change, showing the robustness of the IASI NH₃ product (not shown).

197 The resulting monthly means of IASI NH₃ columns from March to May 2011 are shown in
198 Figure 1 (a to c). The spatio-temporal variability -with the highest values over northeastern
199 France in March, and over northwestern France in April- is confirmed by the IASI 10-year
200 and by the CrIS 5-year monthly means shown in Viatte et al. [2020]. Note that the potential of
201 IASI to provide information at high temporal resolution, up to daily scale, can be hampered
202 by the cloud coverage as only observations with a cloud coverage lower than 10% are
203 delivered [Van Damme et al., 2017]. To evaluate the impact of this limitation, the number of
204 IASI super-observations used to calculate these monthly means, which represents the number
205 of days over a month covered by IASI, is shown in Figure 1 (d to f). On average, more than
206 half of the month is sampled by IASI during spring, except in May in the northwestern part of
207 France. The regions showing large IASI NH₃ values are consequently well sampled.



208

209 **Figure 1.** (top) Monthly means of IASI "super-observations" for (a) March 2011, (b) April
210 2011 and (c) May 2011. Units are molec.cm^{-2} . (bottom) Total number of IASI super-
211 observations per month in (d) March 2011, (e) April 2011 and (f) May 2011.

212 2.2.3. Deducing NH_3 SAT emissions

213 Relative differences between simulated columns by the CHIMERE regional CTM (described
214 in Section 2.2.1, using the TNO-GEN emissions for the year 2011, described in Section 2.1)
215 and observed IASI total columns (described in Section 2.2.2) are applied as a corrective factor
216 to the reference emissions at daily and at grid-cell resolutions over France, from February to
217 May 2011. As IASI "super-observations" provide one piece of information per day, the
218 diurnal time profile of reference emissions cannot be improved: we apply the same daily
219 correction factor to all hourly NH_3 emissions. When IASI is not selected (i.e., observations
220 with a cloud coverage higher than 10%), the correction is not applied and the emissions
221 remain equal to the TNO-GEN ones. To compare the emissions with the CADASTRE-CIT
222 inventory, and their respective simulations with CHIMERE, the correction is only applied
223 over France here.



224 With the mass-balance approach, the transport to neighboring cells is assumed negligible
225 following Palmer et al., [2003]. This approach has been debated by Turner et al. [2012], who
226 found that non-local sources contribute substantially to columns of short-lived species. Li et
227 al. [2019] evaluated the ability of both a mass-balance approach and a variational assimilation
228 to recover known NH_3 emissions at different spatial resolutions. At a $2^\circ \times 2.5^\circ$ resolution, they
229 found that both methods yielded similar values. At a $0.25^\circ \times 0.3125^\circ$, the mass-balance
230 approach led to values about 20% higher compared to the variational ones. With our
231 $0.5^\circ \times 0.25^\circ$ resolution, the use of a mass-balance approach would lead to additional errors of
232 less than about 20% for the quantification of NH_3 emissions. This uncertainty is acceptable
233 and much lower than the uncertainty existing in the annual and national budgets provided by
234 emission inventories [EMEP//EEA, 2016]. In this context, we choose to perform such mass-
235 balance approach to deduce NH_3 emissions from IASI ANNI- NH_3 -v2.2R super-observations.
236 Additional uncertainty comes from the IASI observations. The IASI minimum detection limit
237 is of about 2-3 ppbv ($\sim 4\text{-}6 \cdot 10^{15}$ molecules. cm^{-2}) [Clarisse et al., 2010]. The signal-to-noise
238 ratio therefore presents better performance for regions with high local concentrations (e.g.,
239 northern part of France, Figure 1) than over low local concentration areas (e.g southern parts
240 of France, Figure 1). There is no available evaluation for the IASI ANNI- NH_3 -v2.2R product
241 used here yet.

242 **2.3. CADASTRE-CIT**

243 As a second alternative, a bottom-up approach was set-up based on the finest national
244 inventories available for anthropogenic sources of ammonia. The CADASTRE_ NH_3
245 framework provides such an inventory for organic and mineral fertilization practices. This is
246 however not the case for the other anthropogenic sources. For livestock emissions, excepted
247 manure field spreading, the less detailed inventory of the French Interprofessional Technical
248 Centre for Studies on Air Pollution CITEPA is used. To meet the objectives of better
249 specialization and temporalization, specific procedures are applied. These inventories are
250 completed by the TNO-GEN inventory for the emissions of the other sectors.

251 2.3.1. Fertilization emissions from CADASTRE_ NH_3

252 The CADASTRE_ NH_3 was implemented in order to represent in a realistic way spatio-
253 temporal variability of French NH_3 emissions due to mineral and organic N fertilization, and
254 is fully described in Ramanantenasoa et al. [2018] and in Génarmont et al. [2018]. It has been
255 constructed through the combined use of two types of resources: the process-based



256 VOLT'AIR model and geo-referenced and temporally explicit databases for soil properties,
257 meteorological conditions and N fertilization.

258 VOLT'AIR is a 1D process-based model predicting NH₃ emissions from N fertilizers on bare
259 soils, from physical, chemical and biological processes [Le Cadre, 2004; Garcia et al., 2012].
260 It incorporates current knowledge on NH₃ volatilization after application of the main types of
261 organic manure and mineral N fertilizers in the field. It takes into account the major factors
262 known to influence NH₃ volatilization in the field, i.e., soil properties, weather conditions,
263 cultural practices and properties of mineral fertilizers and organic products. It runs at an
264 hourly time step at the field scale for a period of several weeks covering thus the entire
265 volatilization duration of fertilization events.

266 Local features are attributed to each simulation units, the Small Agricultural Regions (SAR):
267 local weather conditions (SAFRAN, Météo-France), the dominant soil type of the SAR from
268 the European Soil Data Center (ESDC), with soil properties provided by the Harmonized
269 World Soil Database (HWSD) of the Food and Agriculture Organization (FAO); areas
270 cultivated in crop year 2010-2011 per crop per region derived from the European Land Parcel
271 Identification System (LPIS, Common Agricultural Policy (CAP) regulations); Nitrogen
272 fertilization management practices are derived from data of the national AGRESTE survey of
273 cultural practices for arable crops and grassland (Department of Statistics and Forecasting of
274 the French Ministry of Agriculture) [AGRESTE, 2014]. All input data required by
275 VOLT'AIR are geographically overlaid and intersected with a Geographical Information
276 System to generate input combinations in each SAR. Each input combination is used as the
277 input data for a virtual 300m x 300m field for a simulation using VOLT'AIR. Exact times and
278 dates of fertilizations are required to run VOLT'AIR, but for the sake of robustness, the
279 statistical analysis of the survey data has been performed on the base of two-week intervals
280 for the date of fertilization. Fertilizations are thus randomly distributed within these two-week
281 intervals in proportion to their respective representation following Ramanantenasoa et al.
282 [2018]. Each simulation of NH₃ emissions is run at an hourly time step for a period of two
283 months, starting one month before the fertilization in order to calculate soil water content at
284 the time of application, and ending one month after fertilization, in order to cover the whole
285 volatilization event.

286 About 160 000 runs with the VOLT'AIR model have been performed over the crop-year
287 2010-11 to produce ammonia emissions per hour, per ha, per crop type, per SAR. Emissions



288 can be aggregated at different spatial and temporal scales. At the spatial scale, they are
289 weighted with the contribution of (i) each N fertilization management applied to each crop in
290 each SAR and (ii) the area of the crop cultivated in the SAR. A procedure allows producing
291 ammonia emissions at the required grid scale for the inventory comparison: it is based on
292 cultivated areas for each crop as the key of desegregation-reaggregation from the SAR to the
293 $0.015625^\circ \times 0.03125^\circ$ grid. At the temporal scale, emissions are aggregated over daily, weekly
294 or monthly bases for the sake of comparison with TNO-GEN and NH_3SAT inventories.
295 Volatilization taking place over several days, from few days to several weeks, one fertilization
296 in one field contributes to ammonia emissions over several days or weeks. Weather conditions
297 effects on overall ammonia emissions is thus the result of both their effects on fertilization
298 timing and their effects on volatilization intensity and dynamics over 30 days from fertilizer
299 application.

300 As they are not available in the agricultural practice survey, N fertilizations of vegetables,
301 fruits, and vines are not accounted for in CADASTRE_ NH_3 : their contribution is minor for
302 France overall, only accounting for 5% of the total agricultural area [AGRESTE, 2010] but
303 are important in particular regions. As the agricultural practice survey does not provide
304 information over Corsica, this inventory is completed by the TNO-GEN inventory over this
305 region (Figure 2).

306 2.3.2 Livestock emissions

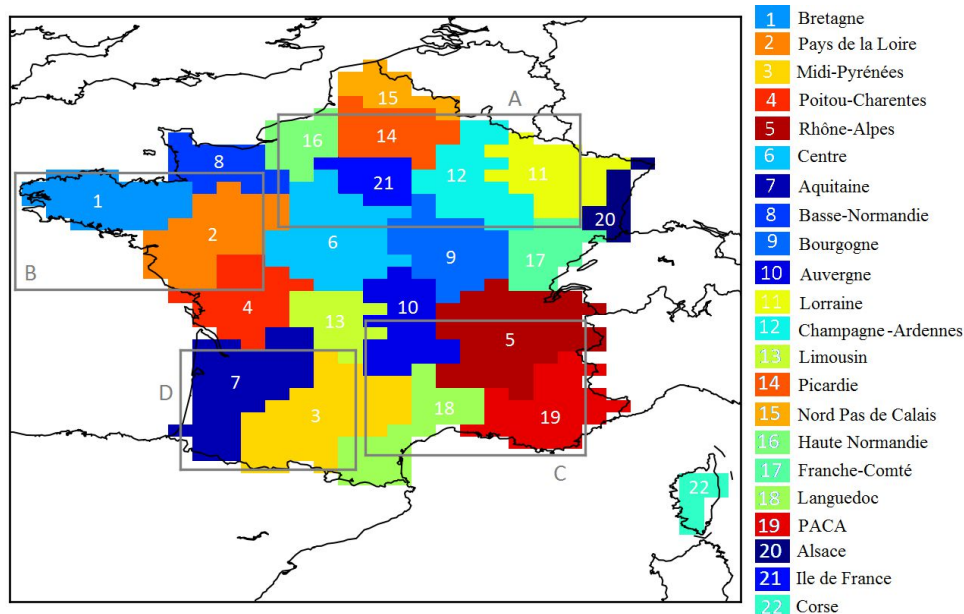
307 As for the TNO-GEN inventory, French NH_3 emissions from livestock for the CADASTRE-
308 CIT inventory are generated by using annual national emissions provided by CITEPA for
309 2011 (Figure 3a). Nevertheless, here these emissions have been spatially distributed
310 differently than for the TNO-GEN inventory. This has been done by using the FAO Gridded
311 Livestock of the World database with a resolution of 30 seconds of arc. The temporalization
312 of the emissions has been performed as a function of temperature and wind speed with the
313 parameterizations of Skøjth et al. [2011] for the different subsectors.

314 **3. Results and discussion**

315 First, we analyze the different contributions of livestock and of fertilization to the spring
316 budget in the CADASTRE-CIT inventory. Then, the comparison of the two alternative
317 inventories NH_3SAT and CADASTRE-CIT versus the reference inventory TNO-GEN, and
318 their inter-comparison are made at different temporal and spatial resolutions. We evaluate the
319 inventories at the national scale and at the scale of the different French administrative



320 regions(the administrative division in France on level 2 of the unified NUTS territory
321 classification, NUTS2, shown in Figure 2). We also analyze their spatial variability at the 0.5°
322 (longitude) x 0.25° (latitude) resolution in order to draw a first picture of the consistency of
323 the inventories in terms of the spring NH_3 total budget and to identify regions of interest.
324 Finally, we focus on the temporal variability of the identified regions and discuss the
325 agricultural practices than can influence the variability but also down to which temporal
326 resolution the comparison of the inventories is relevant.
327



328
329 **Figure 2.** Localization and names of the different French regions as taken into account in this
330 study. The regions are listed according to the TNO-GEN annual budget, in descending order.
331 The grey boxes A, B, C, D describe the domains we respectively call the north-eastern, north-
332 western, south-eastern and south-western parts of France in the following.

333

334 3.1. Respective contributions of different sources

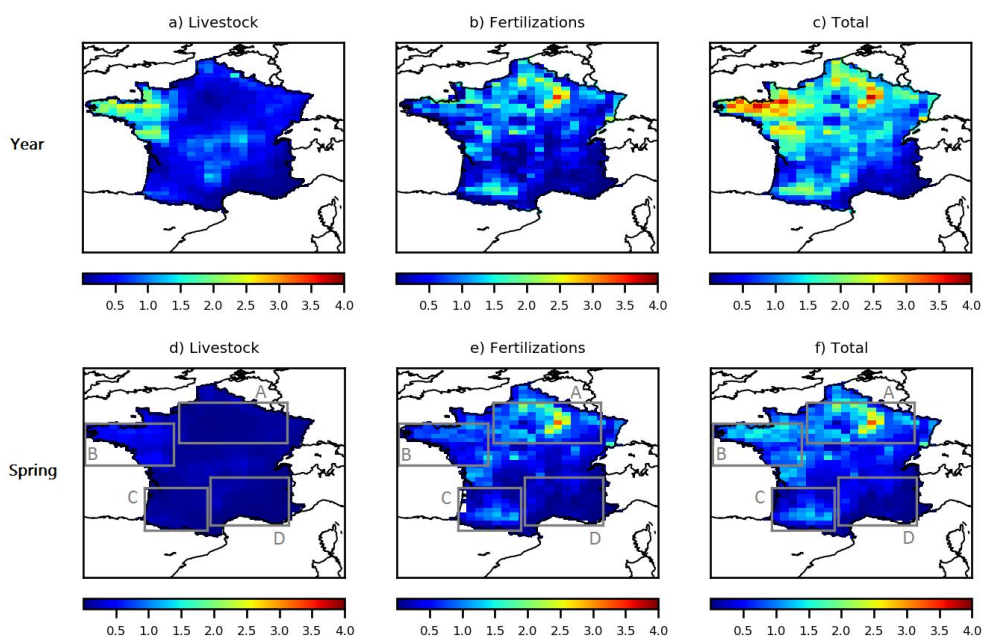
335 The different contributions of livestock and of fertilization to the annual and to the spring
336 budget in the CADASTRE-CIT inventory are shown in Figure 3. This figure shows that the
337 contribution of fertilization to the annual French budget can be strong, with emissions
338 occurring mainly during spring.



339 The different contributions of livestock and of fertilization to the spring budget in the
340 CADASTRE-CIT inventory highlight four different domains of interest. We can see that the
341 contribution of fertilization on the high emissions of the northeastern part of France (box A) is
342 strong. For example, the contribution of fertilization is about 99% in the region Champagne-
343 Ardennes, and about 85% in the region Picardie (Table 2). These emissions are mainly due to
344 the use of mineral fertilizer over barley, sugar beet, and potato [Ramanantenasoa et al., 2018;
345 Générmont et al., 2018]. In particular, the use of urea or nitrogen solution and the high soil
346 pH [Hamaoui-Laguel et al., 2014; Ramanantenasoa et al., 2018; Générmont et al., 2018] -
347 parameters not taken into account by the TNO-GEN inventory- seem to be the factors
348 responsible for the high emissions in this domain.

349 The second domain of interest is the northwestern part of France (box B in Figure 3). Over
350 this domain with high emissions, the NH_3 emissions are due in roughly equal parts to
351 livestock (including animal housing, manure storage, and grazing) and to fertilizations, with a
352 high use of organic manure [Ramanantenasoa et al., 2018]. Livestock farming indeed
353 produces large amounts of livestock manure available for application on grassland and on
354 arable crop.

355 The third domain of interest is the southeastern part of France (box C), showing the smallest
356 spring NH_3 emissions. Finally, the contribution of fertilization on the emissions of the
357 southwestern part of France (box D) is strong.



358

359 **Figure 3.** *top) Yearly NH_3 emissions due to a) livestock husbandry and manure storage, b) N*
360 *fertilization (organic and mineral) and c) all sources in the CADASTRE-CIT inventory, in*
361 *kt NH_3 . bottom) the same for spring NH_3 emissions, from March to May 2011.*

362

363 3.2. French spring NH_3 total budget and its main spatial features

364 The spring NH_3 total budget is shown in Table 2 at the national scale and at the French
365 regional scale. The French spring ammonia budgets, calculated for the period from March to
366 May 2011, estimated by the NH_3SAT (264 kt NH_3) and the CADASTRE-CIT (354 kt NH_3)
367 inventories are both higher than the TNO-GEN reference one (234 kt NH_3). The CADASTRE-
368 CIT inventory estimates higher NH_3 spring emissions, by about 30%, than NH_3SAT .

369

370 The relative agreement on national budget between TNO-GEN and NH_3SAT must be
371 nuanced as total budget values from NH_3SAT and TNO-GEN are close but large differences in
372 the spatial distribution of the French NH_3 emissions between TNO-GEN and both NH_3SAT
373 and CADASTRE-CIT can be observed (Figure 4).

374

375

376

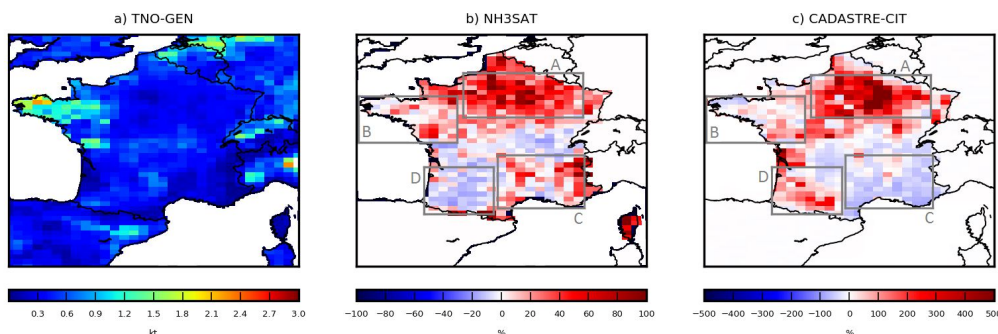


	TNO-GEN (in ktNH ₃)	NH ₃ SAT (in ktNH ₃)	CADASTRE-CIT (in ktNH ₃)	Contribution of the fertilization to the spring budget in CADASTRE-CIT (in %)
Regions in the northeastern part of France (box A in Figure 2)				
Champagne-Ardennes	8	13 (+63%)	35 (+337%)	99
Centre	13	15 (+15%)	32 (+146%)	81
Lorraine	9	12 (+33%)	17 (+88%)	80
Picardie	8	12 (+50%)	30 (+275%)	85
Haute-Normandie	7	9 (+28%)	12 (+71%)	75
Ile de France	3	4 (+33%)	9 (+200%)	77
Regions in the northwestern part of France (box B in Figure 2)				
Bretagne	34	34 (=)	30 (-12%)	61
Pays de la Loire	25	28 (+12%)	29 (+16%)	45
Regions in the southeastern part of France (box C in Figure 2)				
Rhône-Alpes	13	14 (+8%)	12 (-8%)	37
Auvergne	12	12 (=)	11 (-8%)	41
Languedoc	5	6 (+20%)	3 (-40%)	53
PACA	5	5 (=)	2 (-60%)	47
Regions in the southwestern part of France (box D in Figure 2)				
Midi-Pyrénées	18	18 (=)	26 (+44%)	60
Aquitaine	12	11 (-8%)	15 (+25%)	50
Other regions				
Alsace	4	5 (+25%)	7 (+175%)	87
Basse-Normandie	11	15 (+36%)	15 (+36%)	68
Bourgogne	11	13 (+18%)	20 (+81%)	55
Franche-Comté	6	6 (=)	8 (+33%)	43
Limousin	8	8 (=)	6 (-25%)	21
Nord-Pas-de-Calais	8	11 (+38%)	10 (+25%)	97
Poitou-Charentes	14	14 (=)	25 (+79%)	63
France				
	234	264 (+13%)	354 (+51%)	67

377 **Table 2.** French national and regional budgets of NH₃ spring emissions, from March to May
 378 2011, in ktNH₃. The relative differences compared to the TNO-GEN are presented between
 379 brackets, in %. Are marked in bold the regions for which the inventories NH₃SAT and
 380 CADASTRE-CIT propose the same sign of relative differences. The contributions of the
 381 fertilization emissions to the NH₃ regional spring budget in the CADASTRE-CIT inventory are
 382 shown in %.



383 Indeed, over France and for the spring budget, the spatial correlation compared to the
384 CADASTRE-CIT inventory, which should better represent the agricultural practices and their
385 spatial distribution, is improved when using the NH₃SAT inventory instead of using TNO-
386 GEN (Pearson correlation coefficient $r=0.78$ with NH₃SAT against $r=0.72$ with TNO-GEN).



387

388 **Figure 4.** a) French NH₃ spring emissions estimated by the TNO-GEN inventory in ktNH₃,
389 and relative differences of b) the NH₃SAT, and c) the CADASTRE-CIT inventories compared
390 to the TNO-GEN inventory, in %, at the pixel resolution, for the period from March to May
391 2011. Note that the scale is different between 4b) and 4c).

392 The northeastern part of France presents the largest difference with the TNO-GEN inventory
393 (48 ktNH₃) for both NH₃SAT and CADASTRE-CIT inventories (65 and 135 ktNH₃,
394 respectively). Indeed, emissions are higher for both inventories compared to TNO-GEN over
395 the Champagne-Ardennes (+337% and +63%, respectively for CADASTRE-CIT and
396 NH₃SAT, Table 3), Picardie (+275%, and +50%, respectively), Centre (+146% and +15%,
397 respectively), Haute-Normandie (+71% and +28%, respectively), Lorraine (+88%, and +33%,
398 respectively) and Ile de France regions (+200%, and +33%, respectively).

399 The northwestern part of France presents the largest NH₃ emissions according to the TNO-
400 GEN inventory (Figure 4a). The TNO-GEN, NH₃SAT and CADASTRE-CIT inventories lead
401 to similar spring budget (68, 73 and 71 ktNH₃, respectively, over this domain).

402 Over the southeastern part of France, the TNO-GEN and NH₃SAT inventories are also in
403 quite good agreement in terms of budget (35 and 37 ktNH₃, respectively, Table 2) but not in
404 terms of spatial distribution (box C in Figure 4). On the contrary, CADASTRE-CIT is about
405 23% lower than TNO-GEN and NH₃SAT (Table 2). One hypothesis to explain the lower NH₃
406 emissions in CADASTRE-CIT is that market gardening is important in this area and not taken



407 into account in the CADASTRE-CIT inventory [Ramanantenasoa et al., 2018; Générumont et
408 al., 2018].

409 Finally, over the southwestern part of France (box D in Figure 4), IASI observations only
410 trigger slight corrections to the TNO-GEN inventory over this area (29 and 30 ktNH₃,
411 respectively) and CADASTRE-CIT is 36% higher than TNO-GEN and NH₃SAT (Table 2).

412 3.3. Temporal variability of the NH₃ emissions at the sub-seasonal scale

413 Monthly regional budgets have been calculated for the three inventories. Figure 5 presents the
414 monthly variability of the NH₃ emissions from February to May 2011 for the four domains of
415 interest presented above. February is only displayed here as a baseline to show the sharp peak
416 of NH₃ emissions in March over some domains. The contribution of the emissions due to
417 livestock in the CADASTRE-CIT spring budget is also given.

418

419 The TNO-GEN inventory shows rather similar NH₃ emissions from March to May for all
420 regions, with a slight maximum in April (Figure 5a), imposed by the used GENEMIS monthly
421 profiles for the temporalization of emissions [Ebel et al., 1997]. On the contrary, over the
422 northeastern part of France, both NH₃SAT and CADASTRE-CIT inventories show a
423 maximum in March, and a decrease until May by about a factor of 1.5 to 2 (Figure 5a). We
424 calculated the monthly contribution of livestock to the NH₃ emissions based on CADASTRE-
425 CIT, which allows one to separate this contribution from the fertilization one. As in Figure 3,
426 Figure 5a confirms that NH₃ emissions are mainly due to fertilization in the northeastern part
427 of France, and shows that the seasonal variation is mainly driven by this contribution, which
428 confirms the hypothesis formulated in introduction. CADASTRE-CIT shows larger values
429 than NH₃SAT which might be partly due to a possible low bias in the IASI observations
430 [Dammers et al., 2017] combined to the fact that the TNO-GEN inventory (negatively biased
431 compared to CADASTRE-CIT) is used as a priori for the mass balance approach with no
432 correction applied to the a priori when IASI observations are not available.

433 To go further in the comparison, we analyzed the daily variability of the NH₃SAT and
434 CADASTRE-CIT inventories -TNO-GEN representing no daily variability (Figure 6). To
435 interpret the results, some limitations of the inventories have to be considered. For NH₃SAT,
436 the corrections applied to the TNO-GEN emissions are only applied for clear-sky conditions
437 when IASI observations are available. In the CADASTRE-CIT, fertilization days are
438 randomly selected within two-week intervals of application extracted from the farm survey



439 analysis [Ramanantenasoa et al., 2018], thus the actual day of fertilization is unknown.
440 However, the NH_3 volatilization is continuous over several days after spreading reducing the
441 uncertainty introduced by this random selection. Moreover, the random selection is made at
442 the field scale (see section 2.3), then spatially averaging at the CHIMERE resolution should
443 also smoothed the random selection effect. Both effects of weather conditions on fertilization
444 timing, on the one hand, and on volatilization intensity and dynamics at the time of
445 application and after application, on the other hand, are realistically produced. Hence, the NH_3
446 volatilization is continuous over several days after spreading introducing additional
447 smoothing.

448 The CADASTRE-CIT inventories presents a high day-to-day variability from March to May
449 2011 (Figure 6a) with several strong maxima of emissions - characteristic of emissions due to
450 fertilizer application and a significant effect of the varying meteorological conditions. Also
451 for NH_3SAT , day-to-day variability is large. However, NH_3SAT and CADASTRE-CIT
452 maxima are not very well correlated. Over the first 15-days in March 2011, the high
453 emissions occurring from the 9th to 16th in CADASTRE-CIT are not reproduced by the
454 NH_3SAT inventory, potentially because of a lack of IASI coverage for this period (only about
455 40% of the domain –Figure 6a). NH_3SAT shows an emission maximum one week earlier
456 from the 1st to 7th. This time gap in emission maxima could be explained by the random
457 selection of fertilization days in CADASTRE-CIT. Over the last 15 days in March 2011 and
458 over the first 15 days in April 2011, the maxima of emissions estimated by NH_3SAT and
459 CADASTRE-CIT are more correlated, (e.g., from 7th to 11th April in CADASTRE-CIT
460 versus from 9th to 11th in NH_3SAT). Finally, CADASTRE-CIT still shows high emissions in
461 the last 15 days of April and in May 2011, particularly related to the use of fertilizer over
462 corn. Despite a good coverage with IASI observations, no specific high emissions are derived
463 from IASI for the same periods.

464 Over the northwestern part of France, the CADASTRE-CIT inventory is in agreement with
465 TNO-GEN, with a slight maximum in April (Figure 5b). The NH_3SAT inventory shows a
466 maximum in March, related to the high emissions seen during the first week of March 2011
467 (Figure 6b). However, the monthly differences are much smaller than for the northeastern part
468 of France. Also for this domain, the day-to-day variabilities provided by CADASTRE-CIT
469 and NH_3SAT are mostly uncorrelated: a strong sharp maximum of emissions during the first
470 week of March 2011 is seen in NH_3SAT -but not reproduced in CADASTRE-CIT (Figure



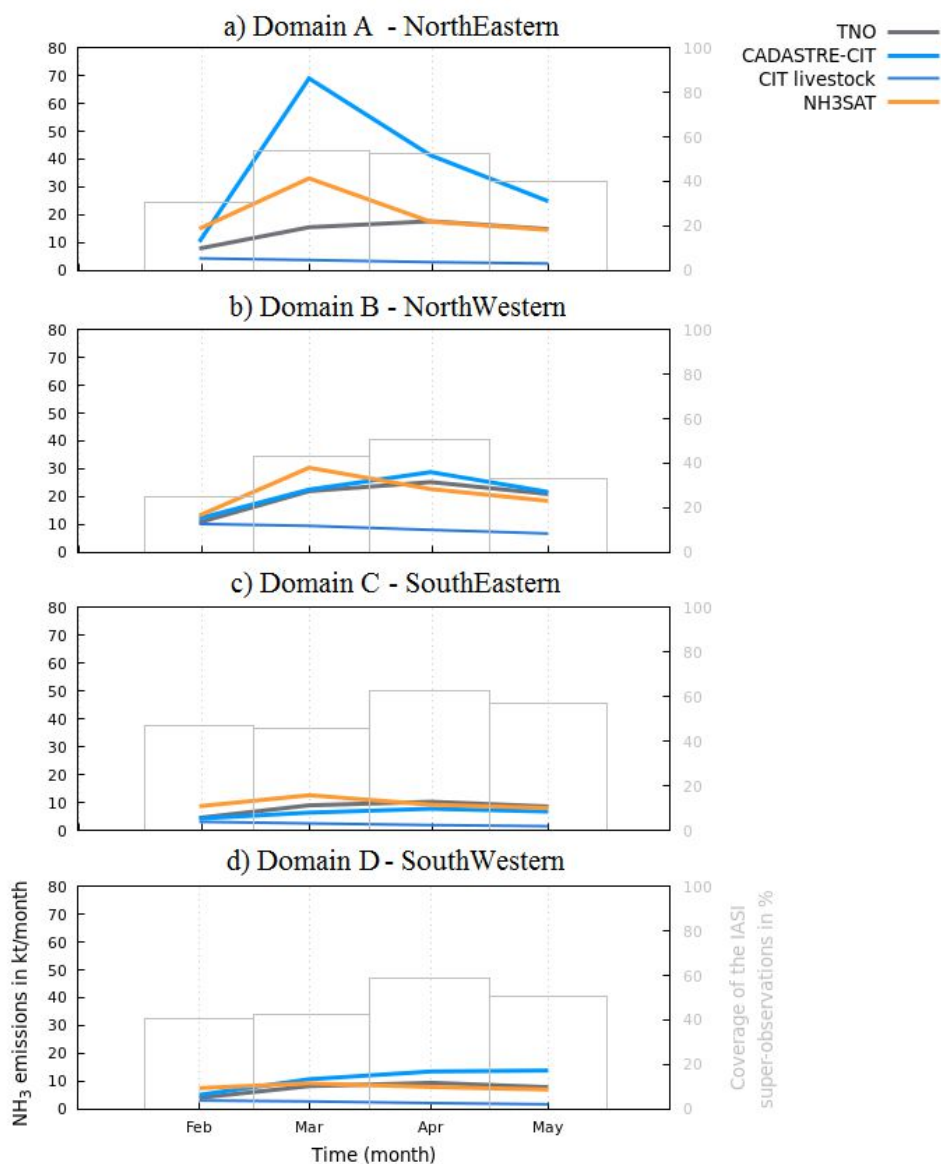
471 6b). The highest daily emissions in CADASTRE-CIT occur during the two last weeks of
472 April 2011 and are not reproduced by NH₃SAT.

473

474 Over the southeastern and southwestern parts of France, month-to-month variations and
475 emission amounts are much smaller than for the two previous domains (Figures 5-6c and
476 Figures 5-6d, respectively). In the southeastern part of France, NH₃SAT emissions are slightly
477 larger than TNO-GEN and CADASTRE-CIT at the beginning of the period (February and
478 March, Figure 5c). The fertilization contribution to CADASTRE-CIT emissions slightly
479 decreases at the end of the period. In the southwestern part of France, NH₃SAT and TNO-
480 GEN are very similar (Figure 5d) and CADASTRE-CIT is slightly larger at the end of spring.
481 This increase is mainly related to fertilization emissions, the livestock contribution being
482 stable. Again, daily time series between both NH₃SAT and CADASTRE-CIT inventories are
483 uncorrelated (Figures 6c, d).

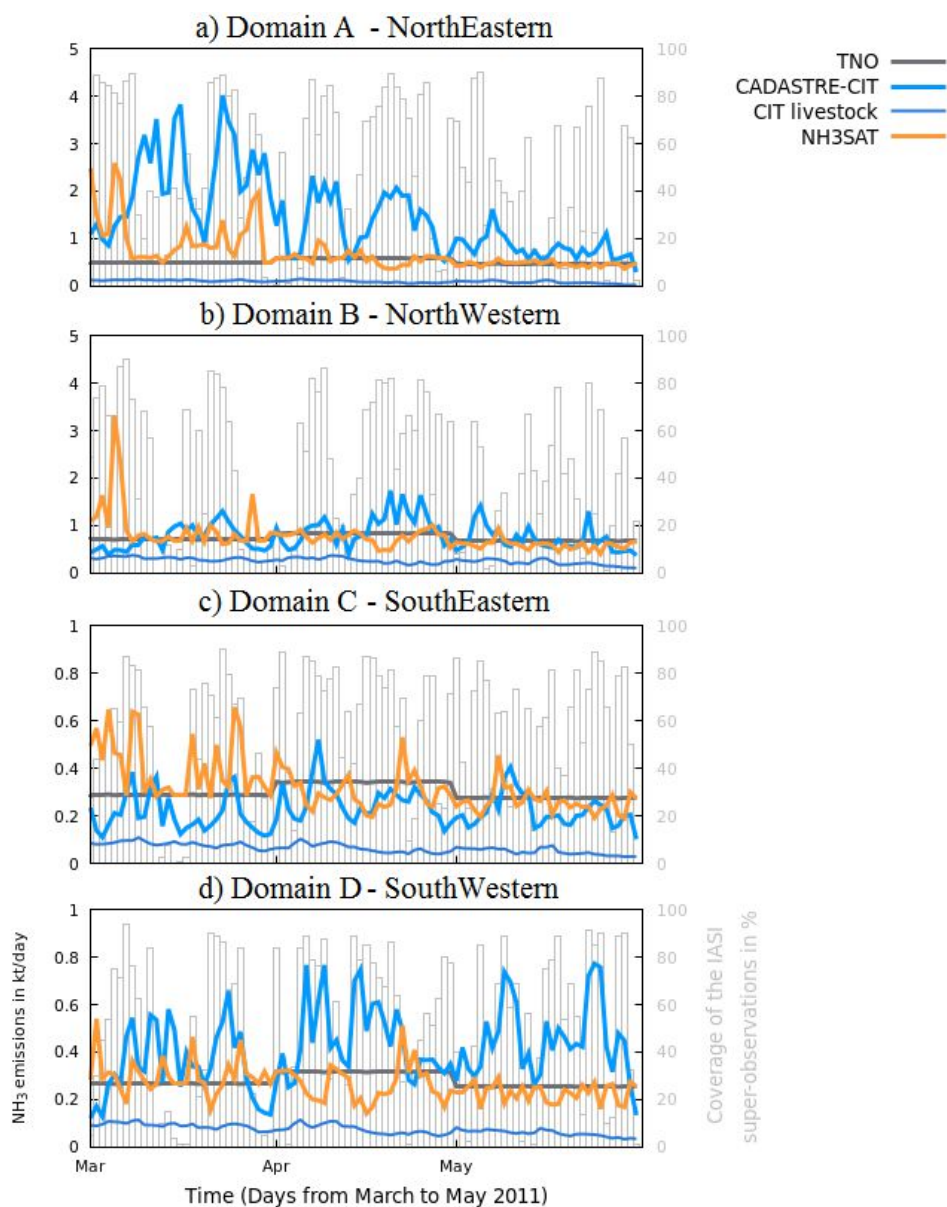
484

485



486

487 **Figure 5.** Time series of monthly NH₃ emissions estimated by TNO-GEN (in grey), by
488 NH₃SAT (in orange), and by CADASTRE-CIT (in blue) inventories, from February to May
489 2011, for (a) domain A (north-eastern), (b) domain B (north-western), (c) domain C (south-
490 eastern), and (d) domain D (south-western), as defined in Figure 2. The contribution of the
491 emissions due to livestock in the CADASTRE-CIT monthly budgets is also given. Units are
492 ktNH₃/month. The monthly regional coverage of the IASI super-observations is given in % (in
493 grey).



494

495 **Figure 6.** Time series of daily NH_3 emissions estimated by TNO-GEN (in grey), by NH_3SAT
496 (in orange), and by CADASTRE-CIT (in blue) inventories, from March to May 2011, for (a)
497 domain A (north-eastern), (b) domain B (north-western), (c) domain C (south-eastern), and
498 (d) domain D (south-western), as defined in Figure 2. Note that the scale is different between
499 a), b) and c), d). Units are ktNH_3/day . The contribution of the emissions due to livestock in the



500 *CADASTRE-CIT daily variability is also given. The daily regional coverage of the IASI super-*
501 *observations is given in % (in grey).*

502 **Conclusion**

503 In this study, we performed an inter-comparison of two alternative inventories with the TNO-
504 GEN reference inventory that quantify the French NH₃ emissions during spring 2011. One of
505 the main conclusion of this study is that over regions with large mineral fertilizer use, like
506 over North-Eastern France, induced NH₃ emissions are probably considerably underestimated
507 by the TNO-GEN reference inventory, as both the NH₃SAT (constrained by IASI
508 observations) and CADASTRE-CIT (process level oriented), show much larger values. For
509 instance, over northeastern France, NH₃SAT and CADASTRE-CIT show respectively a factor
510 1.4 and 2.8 larger spring 2011 emissions than TNO-GEN. Over the whole France, NH₃
511 emissions are still more than 50% larger in CADASTRE-CIT than in TNO-GEN. Average
512 French NH₃SAT emissions are about 10% larger than TNO-GEN ones. Over the southern part
513 of France, with a more diverse agriculture as compared to the crop intensive one in North-
514 eastern France, differences between the inventories are on the whole lower, and signs between
515 CADASTRE-CIT / TNO-GEN and NH₃SAT / TNO-GEN corrections are often opposite for
516 different regions.

517

518 Month-to-month variations are again much more pronounced over North-Eastern France and
519 show a maximum in March for both CADASTRE-CIT and NH₃SAT. Day-to-day variations
520 are large in CADASTRE-CIT and NH₃SAT, roughly a factor of 5 between minimal and
521 maximal values. This shows the interest in evaluating NH₃ emissions at a daily scale because
522 this input is required for chemistry transport modeling of particulate matter formation and
523 thus air quality. However, time-series delivered by CADASTRE-CIT and NH₃SAT are
524 uncorrelated for all considered regions. This result can be partly explained by the lack in IASI
525 NH₃ column observations under partially cloudy conditions, and by the fact that available
526 information on agricultural practices is resolved at a two weeks scale.

527

528 Thus, as a general conclusion, use of observational constrained or process oriented emission
529 inventories is clearly of added-value for estimating better monthly averages over French areas
530 with intensive mineral fertilizer use, but capacity for delivering day-to-day variations is not
531 yet proven. This warrants further studies, both refining hypotheses on days chosen by farmers
532 for fertilizer spread out as a function of meteorological conditions, and, acquiring and using



533 continuous surface NH₃ measurements for validating satellite or process derived NH₃
534 emission variability.

535

536 **Competing interests**

537 The authors declare that they have no conflict of interest.

538 **Author Contribution**

539 All authors have contributed to the manuscript writing (main authors A.F-C, G.D, S.G and
540 MB). A.F-C has performed the mass-balance approach to deduce NH₃ emissions from NH₃
541 total columns observed by the IASI satellite instrument. K.D, J-M.G and S.G have performed
542 the bottom-up approach providing the CADASTRE_NH₃ inventory for organic and mineral
543 fertilization practices. F.C has compiled this CADASTRE_NH₃ inventory with livestock
544 emissions from the CITEPA. L.C, P-F.C, M.V.D and C.C are the PIs of the IASI NH₃
545 product. All authors discussed the results and contributed to the final paper.

546 **Code and Data Availability**

547 The CHIMERE code is available here: www.lmd.polytechnique.fr/chimere/.

548 The IASI ANNI-NH₃-v2.2R data are freely available through the AERIS database:
549 <https://iasi.aeris-data.fr/nh3/>.

550 **Acknowledgements**

551 For this study, A. Fortems-Cheiney and K. Dufossé were funded respectively by the Amp'Air
552 and the PoIQA Primequal projects, under agreement numbers ADEME 1660C0013 and
553 1662C0023, respectively. L.C and M.V.D are respectively research associate and postdoctoral
554 researcher with the Belgian F.R.S-FNRS. The authors are indebted to all those who provided
555 input data for CADASTRE_NH₃ 2010-11 crop year: the *Service de la Statistique et de la*
556 *Prospective* (SSP), Department of Statistics and Forecasting of the French Ministry of
557 Agriculture, for the French cultural practices survey, supported by a public grant overseen by
558 the French National Research Agency (ANR) as part of the "Investissements d'avenir"
559 program (reference: ANR-10-EQPX-17 – *Centre d'Accès Sécurisé aux Données* – CASD);
560 Météo-France for the data on weather conditions; the *Agence de Service et de Paiement* (ASP)
561 and the *Observatoire du Développement Rural* (ODR) service unit for data on Land Parcel
562 Identification System (LPIS) for France. The authors are also grateful to
563 M.M.J. Ramanantenasoa for her technical assistance, funded by the Cadastre_NH₃ project
564 under agreement number ADEME 1081C0031. IASI is a joint mission of EUMETSAT and
565 the Centre National d'Etudes Spatiales (CNES, France). The authors acknowledge the AERIS



566 data infrastructure for providing access to the IASI data in this study. This research has been
567 supported by the Belgian State Federal Office for Scientific, Technical and Cultural Affairs
568 (Prodex arrangement IASI.FLOW). This work was granted access to the HPC resources of
569 TGCC under the allocation A0050107232 made by GENCI.

570 **References**

571 Adams, C., McLinden, C. A., Shephard, M. W., Dickson, N., Dammers, E., Chen, J.,
572 Makar, P., Cady-Pereira, K. E., Tam, N., Kharol, S. K., Lamsal, L. N., and Krotkov, N. A.:
573 Satellite-derived emissions of carbon monoxide, ammonia, and nitrogen dioxide from the
574 2016 Horse River wildfire in the Fort McMurray area, *Atmos. Chem. Phys.*, 19, 2577–2599,
575 <https://doi.org/10.5194/acp-19-2577-2019>, 2019.

576 AGRESTE Pratiques culturelles 2006. In “Agreste Les Dossiers”, n°8- July 2010,
577 pp.86, 2010.

578 AGRESTE Enquête Pratiques culturelles 2011. In “Agreste Les Dossiers”, n°21- July
579 2014, pp.70, 2014.

580 Bauer, S. E., Tsigaridis, K., and Miller, R.: Significant atmospheric aerosol pollution
581 caused by world food cultivation, *Geophys. Res. Lett.*, 43, 5394–5400, 2016.

582 Boersma K. F., Jacob D. J., Bucsele E. J., Perring A. E., Dirksen R., van der A R. J.,
583 Yantosca R. M., Park R. J., Wenig M. O., & Bertram T. H.: Validation of OMI tropospheric
584 NO₂ observations during INTEX-B and application to constrain NO_x emissions over the
585 eastern United States and Mexico. *Atmospheric Environment*, 42(19), 4480–4497.
586 10.1016/j.atmosenv.2008.02.004, 2008.

587 CITEPA, Centre Interprofessionnel Technique d'Etudes de la Pollution Atmosphérique,
588 Format SECTEN, <https://www.citepa.org/fr/air-et-climat/polluants/aep-item/ammoniac>, last
589 access September 2019.

590 Clarisse, L., Shephard, M., Dentener, F., Hurtmans, D., Cady-Pereira, K., Karagulian,
591 F., Van Damme, M., Clerbaux, C., and Coheur, P.-F.: Satellite monitoring of ammonia: A
592 case study of the San Joaquin Valley, *J. Geophys. Res.*, 115, D13302,
593 <https://doi.org/10.1029/2009JD013291>, 2010.

594 Clerbaux, C., Boynard, A., Clarisse, L., George, M., Hadji-Lazarou, J., Herbin, H.,
595 Hurtmans, D., Pommier, M., Razavi, A., Turquety, S., Wespes, C., and Coheur, P.-F.:



596 Monitoring of atmospheric composition using the thermal infrared IASI/MetOp sounder,
597 Atmos. Chem. Phys., 9, 6041–6054, doi:10.5194/acp-9-6041-2009, 2009.

598 Dammers, E., Shephard, M. W., Palm, M., Cady-Pereira, K., Capps, S., Lutsch, E.,
599 Strong, K., Hannigan, J. W., Ortega, I., Toon, G. C., Stremme, W., Grutter, M., Jones, N.,
600 Smale, D., Siemons, J., Hrpcek, K., Tremblay, D., Schaap, M., Notholt, J., and Erisman, J.
601 W.: Validation of the CrIS fast physical NH₃ retrieval with ground-based FTIR, Atmos. Meas.
602 Tech., 10, 2645–2667, <https://doi.org/10.5194/amt-10-2645-2017>, 2017.

603 Dammers, E., McLinden, C. A., Griffin, D., Shephard, M. W., Van Der Graaf, S.,
604 Lutsch, E., Schaap, M., Gainairu-Matz, Y., Fioletov, V., Van Damme, M., Whitburn, S.,
605 Clarisse, L., Cady-Pereira, K., Clerbaux, C., Coheur, P. F., and Erisman, J. W.: NH₃ emissions
606 from large point sources derived from CrIS and IASI satellite observations, Atmos. Chem.
607 Phys., 19, 12261–12293, <https://doi.org/10.5194/acp-19-12261-2019>, 2019.

608 Ebel, A., Friedrich, R., and Rodhe, H.: Tropospheric Modelling and Emission
609 Estimation. Transport and Chemical Transformation of Pollutants in the Troposphere, chap.
610 GENEMIS: Assessment, Improvement, and Temporal and Spatial Disaggregation of
611 European Emission Data, Springer, Berlin, Germany, 1997.

612

613 EEA European Environment Agency: Effects of air pollution on European ecosystems
614 - Past and future exposure of European freshwater and terrestrial habitats to acidifying and
615 eutrophying air pollutants, <https://www.eea.europa.eu/publications/effects-of-air-pollution-on->
616 Technical Report, 2014.

617

618 EMEP European Monitoring and Evaluation Program/EEA European Environment
619 Agency, 2016, Air pollutant emission inventory guidebook Uncertainties, 2016.

620

621 Erisman, J.W. and Schaap, M.: The need for ammonia abatement with respect to
622 secondary PM reductions in Europe, Environ. Pollut., 129, 159–163,
623 <https://doi.org/10.1016/j.envpol.2003.08.042>, 2004.

624

625 Erisman, J.W., Bleeker, A., Galloway, J., and Sutton, M.S.: Reduced nitrogen in
626 ecology and the environment, Environ. Pollut., 150, 1, 140-149,
627 <https://doi.org/10.1016/j.envpol.2007.06.033>, 2007.

628



629 Fortems-Cheiney A., Dufour, G., Hamaoui-Laguel, L., Foret, G., Siour, G., Van
630 Damme, M., Meleux, F., Coheur, P.-F., Clerbaux, C., Clarisse, L., Wallash, M. and
631 Beekmann, M.: Unaccounted variability in NH₃ agricultural sources detected by IASI
632 contributing to European spring haze episode, *Geophysical Research Letters*, 43, 10, 5475–
633 5482, <https://doi.org/10.1002/2016GL069361>, 2016.

634
635 Garcia, L., Générumont, S., Bedos, C., Simon, N. N., Garnier, P., Loubet, B., and
636 Cellier, P.: Accounting for Surface Cattle Slurry in Ammonia Volatilization Models: The
637 Case of Volt'Air. *Soil Science Society of America Journal*, 76, 2184.
638 DOI:10.2136/sssaj2012.0067, 2012.

639 Générumont, S., Ramanantenasoa, M.M.J., Dufossé, K., Maury, O., Mignolet, C.,
640 Gilliot, J.-M. : Data on spatio-temporal representation of mineral N fertilization and manure N
641 application as well as ammonia volatilization in French regions for the crop year 2005/06,
642 Data in Brief 21:1119-1124. <https://doi.org/10.1016/j.dib.2018.09.119>, 2018.

643 Hamaoui-Laguel, L., Meleux, F., Beekmann, M., Bessagnet, B., Générumont, S.,
644 Cellier, P., Letinois, L.: Improving ammonia emissions in air quality modelling for France.
645 *Atmospheric Environment*, 92, 584–595, doi: 10.1016/j.atmosenv.2012.08.002, 2014.

646 Hellsten, S., U. Dragosits, C.J. Place, M. Vieno, J. Dore, T.H. Misselbrook, Y.S. Tang,
647 M.A. Sutton: Modelling the spatial distribution of ammonia emissions in the UK,
648 *Environmental Pollution (Barking, Essex: 1987)*, 154 (2008), pp. 370–379, 2008.

649 Jaeglé, L., R. V. Martin, K. Chance, L. Steinberger, T. P. Kurosu, D. J. Jacob, A. I.
650 Modi, V. Yoboué, L. Sigha-Nkamdjou, and C. Galy-Lacaux, Satellite mapping of rain-
651 induced nitric oxide emissions from soils, *J. Geophys. Res.*, 109, D21310,
652 doi:10.1029/2004JD004787, 2004.

653 Kuenen, J. J. P., Visschedijk, A. J. H., Jozwicka, M., and Denier van der Gon, H. A.
654 C.: TNO-GEN-MACC_II emission inventory; a multi-year (2003–2009) consistent high-
655 resolution European emission inventory for air quality modelling, *Atmos. Chem. Phys.*, 14,
656 10963-10976, <https://doi.org/10.5194/acp-14-10963-2014>, 2014.

657 Le Cadre, E. : "Modélisation de la volatilisation d'ammoniac en interaction avec les
658 processus chimiques et biologiques du sol: le modèle Volt'Air." Doctoral thesis, ABIES ;
659 UMR INRA INAPG Environnement et Grandes Cultures de Grignon. pp. 315., 2004.
660 http://infodoc.agroparistech.fr/index.php?lvl=notice_display&id=48284



- 661 Lelieveld, J., Evans, J.S., Fnais, M., Giannadaki, D. and Pozzer, A.: The contribution
662 of outdoor air pollution sources to premature mortality on a global scale, *Nature*, 367-371,
663 doi:10.1038/nature15371, 2015.
- 664 Li et al: Assessing the iterative finite difference mass balance and 4D-Var methods to
665 derive ammonia emissions over North America using synthetic observations, *J. Geoph.*
666 *Res.*,<https://doi.org/10.1029/2018JD030183>, 2019.
- 667 Lin, J. T., M. B. McElroy, and K. F. Boersma: Constraint of anthropogenic NO_x
668 emissions in China from different sectors: A new methodology using multiple satellite
669 retrievals, *Atmos. Chem. Phys.*, 10, 63–78, doi:10.5194/acp-10-63-2010, 2010.
- 670 Mailler, S., Menut, L., Khvorostyanov, D., Valari, M., Couvidat, F., Siour, G.,
671 Turquety, S., Briant, R., Tuccella, P., Bessagnet, B., Colette, A., Létinois, L., Markakis, K.,
672 and Meleux, F.: CHIMERE-2017: from urban to hemispheric chemistry-transport modeling,
673 *Geosci. Model Dev.*, 10, 2397–2423, <https://doi.org/10.5194/gmd-10-2397-2017>, 2017.
- 674 Menut, L., Goussebaile, A., Bessagnet B., Kyvorostyanov, D., and Ung, A.: Impact of
675 realistic hourly emissions profiles on air pollutants concentrations modelled with CHIMERE,
676 *Atmospheric Environment*, 49, 233-244, 2012.
- 677 Menut, L., Bessagnet, B., Khvorostyanov, D., Beekmann, M., Blond, N., Colette, A.,
678 Coll, I., Curci, G., Foret, G., Hodzic, A., Mailler, S., Meleux, F., Monge, J.-L., Pison, I.,
679 Siour, G., Turquety, S., Valari, M., Vautard, R., and Vivanco, M. G.: CHIMERE 2013: a
680 model for regional atmospheric composition modelling, *Geosci. Model Dev.*, 6, 981-1028,
681 doi:10.5194/gmd-6-981-2013, 2013.
- 682 Nenes, A., Pandis, S.N., and Pilinis, C.: Continued development and testing of a new
683 thermodynamic aerosol module for urban and regional air quality models, *Atmospheric*
684 *Environment*, 33, 1553–1560, 1999.
- 685 OJEU, Official Journal of the European, Union Directive (EU) 2016/2284 of the
686 European Parliament and of the Council of 14 December 2016 on the reduction of national
687 emissions of certain atmospheric pollutants, amending Directive 2003/35/EC and repealing
688 Directive 2001/81/EC, 344, 17.12.2016, p. 1–31, <http://data.europa.eu/eli/dir/2016/2284/oj>,
689 2016.
- 690 Owens, R. G. and Hewson, T.: ECMWF Forecast User
691 Guide,<https://doi.org/10.21957/m1cs7h>, 2018.



692 Palmer, P.I., Jacob, D.J., Fiore, A.M., Martin, R.V., Chance, K., and Kurosu, T.P.:
693 Mapping isoprene emissions over North America using formaldehyde column observations
694 from space, *J. Geophys. Res.*, 108, D6, doi:10.1029/2002JD002153, 2003.

695 Ramanantenasoa M.M.J., Gilliot J.-M., Mignolet C., Bedos C., Mathias E., Eglin T.,
696 Makowski D., Générumont S.: A new framework to estimate spatio-temporal ammonia
697 emissions due to nitrogen fertilization in France. *Science of the Total Environment*, 645:205-
698 219. <https://doi.org/10.1016/j.scitotenv.2018.06.202>, 2018.

699 Schauburger, B et al: Yield trends, variability and stagnation analysis of major crops in
700 France over more than a century, *Nature*, doi:10.1038/s41598-018-35351-1, 2018.

701 Skjøth, C. A., Geels, C., Berge, H., Gyldenkærne, S., Fagerli, H., Ellermann, T.,
702 Frohn, L. M., Christensen, J., Hansen, K. M., Hansen, K., and Hertel, O.: Spatial and
703 temporal variations in ammonia emissions – a freely accessible model code for Europe,
704 *Atmos. Chem. Phys.*, 11, 5221-5236, doi:10.5194/acp-11-5221-2011, 2011.

705 Szopa, S., Foret, G., Menut, L., and Cozic, A.: Impact of large scale circulation on
706 European summer surface ozone: consequences for modeling, *Atmospheric Environment*, 43,
707 1189–1195, doi:10.1016/j.atmosenv.2008.10.039, 2008.

708 Turner, A.J., Henze, D.F., Martin, R.V. and Hakami, A.: The spatial extent of source
709 influences on modeled columns concentrations of short-lived species, *Geophysical Research*
710 *Letters*, 39, L12806, doi:10.1029/2012GL051832, 2012.

711 Van Damme, M., Clarisse, L., Heald, C. L., Hurtmans, D., Ngadi, Y., Clerbaux, C.,
712 Dolman, A. J., Erisman, J. W., and Coheur, P. F.: Global distributions, time series and error
713 characterization of atmospheric ammonia (NH₃) from IASI satellite observations, *Atmos.*
714 *Chem. Phys.*, 14, 2905–2922, doi:10.5194/acp-14-2905-2014, 2014.

715 Van Damme, M., Whitburn, S., Clarisse, L., Clerbaux, C., Hurtmans, D., and Coheur,
716 P.-F.: Version 2 of the IASI NH₃ neural network retrieval algorithm: near-real-time and
717 reanalysed datasets, *Atmos. Meas. Tech.*, 10, 4905-4914, [https://doi.org/10.5194/amt-10-](https://doi.org/10.5194/amt-10-4905-2017)
718 4905-2017, 2017.

719 Van Damme, M., Clarisse, L., Whitburn, S., Hadji-Lazaro, J., Hurtmans, D., Clerbaux,
720 C., and Coheur, P.-F.: Industrial and agricultural ammonia point sources exposed, *Nature*,
721 Volume 564, 99-103, 2018.



722 Vestreng, V., Breivik, K., Adams, M., Wagner, A., Goodwin, J., Rozovskaya, O., and
723 Oacyna, J. . Inventory Review 2005 - Emission Data reported to CLRTAP and under the NEC
724 Directive - Initial review for HMs and POPs .EMEP Status report, Norwegian Meteorological
725 Institute, Oslo, 2005.

726
727 Viatte, C., Wang, T., Van Damme, M., Dammers, E., Meleux, F., Clarisse, L.,
728 Shephard, M. W., Whitburn, S., Coheur, P. F., Cady-Pereira, K. E., and Clerbaux, C.:
729 Atmospheric ammonia variability and link with particulate matter formation: a case study
730 over the Paris area, *Atmos. Chem. Phys.*, 20, 577–596, [https://doi.org/10.5194/acp-20-577-](https://doi.org/10.5194/acp-20-577-2020)
731 2020, 2020.

732 Zhu, L., Henze, D.K., Cady-Pereire, K.E, Shepard, M.W., Luo, M., Pinder, R.W.,
733 Bash, J.O. and Jeong, G.-R.: Constraining U.S. ammonia emissions using TES remote sensing
734 observations and the GEOS-Chem adjoint model, *J. Geophys. Res.*, 118, 1-14,
735 doi:10.1002/jgrd.50166, 2013.

736